

Where the Quantum Lives in D-Wave Hybrid Portfolio Optimization: An Operational Decomposition Audit

Luis Lozano*

*EGADE Business School, Tecnológico de Monterrey,
Santa Fe, Mexico City, Mexico*

Abstract

We audit the operational decomposition of D-Wave’s hybrid quantum-classical portfolio-optimization service on cardinality-constrained mean-variance-turnover instances spanning $N=10$ to 640, with the constraint-native LeapHybridCQM interface, the penalty-encoded LeapHybridBQM interface, and Gurobi MIQP and simulated-annealing classical anchors. We report all three SDK timing fields (t_{run} , t_{charge} , t_{QPU}) and define a candidate four-metric audit protocol for hybrid quantum-classical solvers. Three findings. First, the LeapHybridCQM service matches Gurobi’s proven optimum on all 54 head-to-head instances at $N \leq 120$, but the mean QPU access time is 0.034 seconds out of the 5-second nominal wall-clock budget — 0.68% of the nominal budget, $\approx 0.72\%$ of measured run time — and the remaining $\sim 99\%$ is the service’s classical decomposition and feasibility-aware reassembly. Second, in a CPU-only matched-wall-clock counterfactual, TabuSampler on the penalty-encoded BQM reaches final exact- K objectives within mean absolute delta 0.001 of hybrid CQM on 24 tested instances; this does not ablate the LeapHybridCQM pipeline internals, but it shows that these objective levels are reproducible by a classical heuristic at the same wall-clock budget. Third, the cardinality penalty contributes a dense rank-one term that fully connects the encoded logical graph independent of the input covariance density, an effect we prove as a structural theorem; the resulting density-axis collapse explains the BQM degradation observed in the empirical comparison. Out-of-sample on Fama–French 49 industry portfolios, the QPU-selected portfolios deliver a mean Sharpe ratio of 1.94 versus 2.22 for the $1/N$ baseline. The practical implication is that reported D-Wave hybrid wins on this problem class are constraint-native classical pipelines, not quantum-sampling wins.

Keywords: portfolio optimization; cardinality constraint; quantum-classical hybrid solver; benchmarking; D-Wave; mean-variance-turnover.

JEL classification: G11; C61; C63.

1 Introduction

Quantum annealing has attracted sustained interest as a potential accelerator for combinatorial portfolio optimization [Orús et al., 2019, Herman et al., 2023]. The standard approach encodes a cardinality-constrained mean-variance objective as a quadratic unconstrained binary optimization (QUBO) problem, adds a quadratic penalty term to enforce the cardinality constraint, embeds the resulting logical graph onto the hardware topology via minor embedding, and samples on the quantum processing unit (QPU) [Venturelli and Kondratyev, 2019, Mugel et al., 2022, Sakuler et al., 2025]. A parallel line of work uses D-Wave’s hybrid cloud solvers,

*e-mail address: 1alozano@tec.mx; ORCID: 0000-0001-7202-3437

which accept either penalty-encoded binary quadratic models (BQMs) or constraint-native constrained quadratic models (CQMs) and allocate classical and QPU resources internally [Mugel et al., 2022].

Despite this body of work, the relative performance of these formulation choices has not been systematically characterized across the joint space of problem size, covariance density, and solver budget. Most studies benchmark a single solver at a single scale. We address this gap by defining a canonical mean-variance-turnover (MVT) portfolio problem and comparing four solver paths (direct QPU, hybrid BQM, hybrid CQM, and classical baselines: Gurobi MIQP and simulated annealing) across controlled synthetic instances and real equity data from the Fama–French 49 industry portfolios [French, 2026]. In practical portfolio rebalancing, turnover is not a cosmetic term: changing positions incurs transaction costs, market impact, and operational frictions. A solver that spends its budget satisfying an artificial cardinality penalty rather than improving the risk-return-turnover objective can produce portfolios whose implementation cost overwhelms the expected return benefit. The intended users of these results are D-Wave practitioners choosing between solver interfaces, fintech engineering teams evaluating hybrid solvers for constrained allocation problems, and quantitative researchers benchmarking quantum-assisted portfolio optimization.

Contributions. This paper makes three principal contributions to the literature on hybrid quantum-classical portfolio optimization. The first is empirical: on the 162 synthetic-hybrid runs of the $N=10$ –640 campaign, the constraint-native LeapHybridCQM service matches Gurobi’s proven optimum on every head-to-head instance where Gurobi proves optimality (54 instances at $N \leq 120$; a paired Wilcoxon signed-rank test rejects equality of paired CQM and BQM objectives at every $N \geq 20$, $p < 0.05$), and we report all three SDK timing fields rather than the single t_{QPU} measurement that has previously been treated as the proxy for “quantum work.” Mean t_{QPU} is 0.034 seconds out of the 5-second hybrid CQM minimum budget — a 0.68% QPU wall-clock fraction — and the service returns bitwise-identical objective values across all available repeated calls at every tested (N, ρ, B) cell.¹

The second contribution is causal-attribution. Because the protocol’s r_{QPU} metric (introduced in the third contribution below) bounds wall-clock share rather than causal contribution, we resolve the attribution question directly with a CPU-only matched-wall-clock counterfactual: `TabuSampler` at 5s on the same penalty-encoded BQM that hybrid BQM consumes, on 24 instances at $N \in \{50, 80, 120, 200\}$. The Tabu objectives match hybrid CQM to within mean absolute delta 0.001 (max 0.008) and match Gurobi to similar tolerance. Because the penalty-encoded BQM and the constraint-native CQM encode the same cardinality-constrained problem (same feasible set, same optimal solution), recovering CQM-matching objectives on the BQM is equivalent to recovering the same portfolio \mathbf{z}^* . Combined with the 0.68% wall-clock fraction, this empirically is consistent with a very small causal quantum-sampling contribution to the share of hybrid CQM solution quality that any quantum contribution could be providing at the tested scales: at matched compute, a classical heuristic alone reaches the same objective levels.

The third contribution is methodological. We formalise the empirical density-axis collapse as a theorem: for any cardinality constraint $\mathbf{1}^\top \mathbf{z} = K$ enforced by quadratic penalty $A \cdot (\mathbf{1}^\top \mathbf{z} - K)^2$, the encoded QUBO matrix has off-diagonal support equal to the complete graph K_N regardless of the input covariance support, with chain-break growth a monotone consequence of the resulting embedding overhead. Building on this structural result, we propose an operational decomposition audit protocol consisting of four metrics — the QPU wall-clock fraction r_{QPU} , the optimality gap g_F , the encoded-graph density amplification d_{amp} , and the service variance v_{service} — and a seven-step reporting procedure for hybrid benchmarks. A reference implementation accompanies the paper. An out-of-sample financial layer on Fama–French 49-industry portfolios further shows

¹10 repetitions completed in every cell except ($N=50$, dense, 300s), where four completed within the campaign wall-clock budget; the determinism observation is verified at the cell level against the saved JSONL records.

that the cardinality-constrained portfolios these solvers return marginally underperform a naive $1/N$ benchmark in Sharpe terms (-0.28 on average across five rolling windows), with the largest positive QPU-minus-baseline spread occurring in the earliest sampled window.

Together, these results reframe what a reported D-Wave hybrid win on this problem class can claim: it is a constraint-native classical pipeline with a small measured QPU-access component, and the operational benchmarking standard should report all three timing fields and explicit matched-compute classical baselines rather than t_{QPU} alone.

This study sits next to several portfolio-optimization benchmarks using quantum and hybrid methods. Mugel et al. [2022] study dynamic portfolio optimization on real data with quantum and quantum-inspired methods. Sakuler et al. [2025] compare QBSolv, Hybrid BQM, Hybrid CQM, and exact classical solutions for a production portfolio-optimization use case, finding that CQM is useful for handling constraints without manual penalty tuning. Lang et al. [2022] and Buonaiuto et al. [2023] benchmark annealing and gate-model workflows for portfolio optimization, while Acharya et al. [2025] develop a decomposition pipeline for large constrained portfolio and rebalancing problems. Morapakula et al. [2025] build an end-to-end deployable pipeline that combines CQM-based discrete asset selection with classical weight allocation and rebalancing, demonstrating the operational viability of hybrid annealing in a real market context. Our contribution is narrower and more diagnostic: we isolate the formulation choice for a mean-variance-turnover problem, sweep size, covariance density, and solver budget, and connect the hybrid BQM/CQM gap to the direct-QPU embedding mechanism.

We note explicitly that this is a formulation-and-platform study within the D-Wave ecosystem, not a broad quantum-vs-classical superiority claim. Classical solvers (Gurobi MIQP) find provably optimal solutions on all tested instances at $N \leq 200$ (the academic license does not support the model size at $N \geq 400$); the practical question addressed here is which D-Wave solver interface to use when a practitioner has chosen to use D-Wave hardware.

My companion paper [Lozano, 2026] addresses the adjacent practitioner question of how to make direct-QPU portfolio optimisation viable by replacing the penalty-encoded QUBO with an objective-only QUBO and a classical feasibility projector. The density-collapse root diagnosis (Theorem 1 below) is common to both; the present paper restricts attention to the existing LeapHybridCQM and LeapHybridBQM service interfaces, while the companion paper builds a custom direct-QPU pipeline. Each paper stands alone.

2 Background

2.1 Cardinality-Constrained Portfolio Selection

The classical mean-variance portfolio problem [Markowitz, 1952] selects asset weights to maximize expected return for a given risk level. Adding a cardinality constraint (select exactly K out of N candidate assets) makes the problem NP-hard in general [Bertsimas and Shioda, 2009, Lucas, 2014] and motivates a long line of mixed-integer quadratic-programming formulations in the OR / finance literature [Bertsimas and Shioda, 2009]. In the binary formulation, each asset i has a selection variable $z_i \in \{0, 1\}$ and the objective is:

$$\min_{z \in \{0,1\}^N} -\boldsymbol{\mu}^\top z + \lambda z^\top \Sigma z \quad \text{s.t.} \quad \mathbf{1}^\top z = K, \quad (1)$$

where $\boldsymbol{\mu}$ is the expected return vector, Σ is the covariance matrix, and $\lambda > 0$ is the risk-aversion parameter.

2.2 Mean-Variance-Turnover Formulation

For repeated re-optimization across consecutive decision periods, we extend (1) with a switching-cost penalty:

$$\min_{z \in \{0,1\}^N} -\boldsymbol{\mu}^\top z + \lambda z^\top \Sigma z + \boldsymbol{\tau}^\top |z - z_{t-1}| \quad \text{s.t.} \quad \mathbf{1}^\top z = K, \quad (2)$$

where z_{t-1} is the previous binary portfolio and $\boldsymbol{\tau}$ is the per-asset switching cost. Because both z and z_{t-1} are binary, the absolute-value term is linear: $|z_i - z_{t-1,i}| = z_i(1 - z_{t-1,i}) + (1 - z_i)z_{t-1,i}$, which absorbs into the QUBO diagonal without introducing auxiliary variables or additional pairwise couplers.

2.3 Penalty-Encoded QUBO (BQM Path)

The standard QUBO encoding promotes the cardinality constraint into the objective via a quadratic penalty:

$$Q_{\text{BQM}} = -\text{diag}(\boldsymbol{\mu}) + \lambda \Sigma + A \cdot \mathbf{1}\mathbf{1}^\top - 2AK \cdot I + \text{diag}(\boldsymbol{\tau}_{\text{shift}}), \quad (3)$$

where $A > 0$ is the penalty weight and $\boldsymbol{\tau}_{\text{shift},i} = \tau_i(1 - 2z_{t-1,i})$. The $A \cdot \mathbf{1}\mathbf{1}^\top$ term makes the QUBO fully connected regardless of the sparsity of Σ , a phenomenon termed *constraint dilution* [Verma and Lewis, 2022, Lozano, 2026]. This full connectivity forces $N(N - 1)/2$ couplers in the logical graph and long minor-embedding chains on hardware topologies with bounded degree.

2.4 Constraint-Native CQM (CQM Path)

D-Wave’s constrained quadratic model (CQM) interface accepts the cardinality constraint natively, eliminating the penalty term entirely:

$$Q_{\text{CQM}} = -\text{diag}(\boldsymbol{\mu}) + \lambda \Sigma + \text{diag}(\boldsymbol{\tau}_{\text{shift}}), \quad \text{constraint: } \mathbf{1}^\top z = K. \quad (4)$$

The CQM objective preserves the sparsity structure of Σ . The hybrid solver handles constraint satisfaction internally through a combination of classical and quantum resources.

2.5 Density-Axis Collapse

A structural consequence of (3) is that the original covariance density ρ of Σ is irrelevant to the encoded logical graph density when using penalty encoding: the $A \cdot \mathbf{1}\mathbf{1}^\top$ term produces a complete graph for any Σ . We formalise this as a theorem.

Theorem 1 (Density-Axis Collapse under Quadratic Penalty Encoding). *Adopt the symmetric QUBO convention $H(z) = z^\top Qz$ with $Q = Q^\top$; under this convention the off-diagonal coefficient of $z_i z_j$ ($i \neq j$) in the Hamiltonian is $2Q_{ij}$. Let $z \in \{0,1\}^N$ and consider a linear equality constraint $\sum_{i=1}^N a_i z_i = b$ with $a \in \mathbb{R}^N$ and $b \in \mathbb{R}$, enforced in QUBO form by the quadratic penalty $A \cdot (\sum_i a_i z_i - b)^2$ added to an objective with symmetric cost matrix $C \in \mathbb{R}^{N \times N}$. Define the off-diagonal support of a matrix M as $\text{supp}_{\text{off}}(M) := \{(i, j) : i < j, M_{ij} \neq 0\}$. Then for every penalty weight A outside the finite set $\{-C_{ij}/(a_i a_j) : i < j, a_i a_j \neq 0\}$,*

$$\text{supp}_{\text{off}}(Q) = \text{supp}_{\text{off}}(C) \cup \{(i, j) : i < j, a_i a_j \neq 0\}. \quad (5)$$

In particular, if $a_i \neq 0$ for all i (e.g., $a = \mathbf{1}$ for an exact-cardinality constraint), then $\text{supp}_{\text{off}}(Q) = \{(i, j) : 1 \leq i < j \leq N\}$ and the logical graph of Q — defined as the graph on $[N]$ with edge set $\{(i, j) : i \neq j, Q_{ij} \neq 0\}$ — is the complete graph K_N .

Proof. Expanding the penalty,

$$A \cdot (a^\top z - b)^2 = A \cdot z^\top (aa^\top) z - 2Ab \cdot a^\top z + Ab^2.$$

The first term contributes $A \cdot a_i a_j$ to the off-diagonal entry Q_{ij} for every $i \neq j$ with $a_i a_j \neq 0$; equivalently, it contributes $2A \cdot a_i a_j$ to the coefficient of $z_i z_j$ in an upper-triangular QUBO convention. The first term also contributes $A \cdot a_i^2$ to Q_{ii} . The second is linear in z and contributes $-2Ab \cdot a_i$ to Q_{ii} . The constant Ab^2 shifts the total energy. Combining with the original off-diagonal contribution from C , we obtain $Q_{ij} = C_{ij} + A \cdot a_i a_j$ for $i \neq j$; this is non-zero whenever $a_i a_j \neq 0$ and $A \neq -C_{ij}/(a_i a_j)$. The exception set, $\{-C_{ij}/(a_i a_j) : i < j, a_i a_j \neq 0\}$, is finite (at most $\binom{N}{2}$ values). For A outside this set, equation (5) holds entry-by-entry. When $a_i \neq 0$ for all i , the second set on the right-hand side equals $\{(i, j) : i < j\}$, which yields the logical-graph claim. \square

In plain terms. The cardinality penalty forces every asset to interact with every other asset through the shared quadratic term, so the encoded problem becomes fully connected even when the original covariance matrix is diagonal. For the cardinality constraint of Section 2, $a = \mathbf{1}$ and $b = K$, and the second set on the right of equation (5) becomes $\{(i, j) : i < j\}$ regardless of $\text{supp}_{\text{off}}(\Sigma)$.

Remark (MVT objective inherits the same collapse). The mean-variance-turnover (MVT) objective of (2) differs from the bare MV objective by a turnover term $\tau^\top |z - z_{t-1}|$. For binary $z, z_{t-1} \in \{0, 1\}^N$, the identity $|z_i - z_{t-1,i}| = z_{t-1,i} + (1 - 2z_{t-1,i})z_i$ holds by enumeration, so the turnover term is linear in z and contributes only to the diagonal of Q . Consequently $\text{supp}_{\text{off}}(Q^{\text{MVT}}) = \text{supp}_{\text{off}}(Q^{\text{MV}})$, and Theorem 1 applies to MVT verbatim.

Remark (CQM path preserves $\text{supp}_{\text{off}}(\Sigma)$). The constraint-native CQM formulation in (4) contains no penalty term; the cardinality constraint is held natively by the solver and does not modify the objective coefficients. Hence the off-diagonal quadratic objective support is $\text{supp}_{\text{off}}(Q_{\text{CQM}}) = \text{supp}_{\text{off}}(\Sigma)$, with no $A \cdot \mathbf{1}\mathbf{1}^\top$ contribution.

Corollary 2 (Embedding-Overhead Lower Bound for K_N on a Bounded-Degree Topology). *Let $G = (V_G, E_G)$ be a hardware topology with maximum vertex degree d . Any minor embedding of K_N into G uses at least $N(N-1)/d$ physical qubits in total across all chains:*

$$L_{\text{tot}} := \sum_{i=1}^N |\text{chain}_i| \geq \frac{N(N-1)}{d}.$$

Equivalently, the per-logical physical-qubit overhead grows at least as $\Omega(N/d)$.

Proof. K_N has $\binom{N}{2}$ logical edges. Each logical edge requires at least one *inter-chain* physical edge — a physical edge in E_G with one endpoint in chain_i and the other in chain_j for the respective logical qubits $i \neq j$; intra-chain edges play no role here, they only further reduce the available degree budget at each physical vertex. Each physical vertex in G has degree at most d , so each physical vertex contributes at most d such inter-chain edges in total. Summing the inter-chain degree contributions across all physical vertices: $L_{\text{tot}} \cdot d$ is at least the total inter-chain endpoint count, which equals $2\binom{N}{2} = N(N-1)$. Rearranging gives the claimed bound. \square

For Pegasus ($d = 15$) at $N = 80$, the bound gives $L_{\text{tot}} \geq 421$ physical qubits. The observed value in Table 1 is 750, consistent with the bound. For Zephyr ($d = 20$) at the same N the bound gives ≈ 316 . Tighter topology-specific constants for Pegasus and Zephyr appear in Boothby et al. [2020].

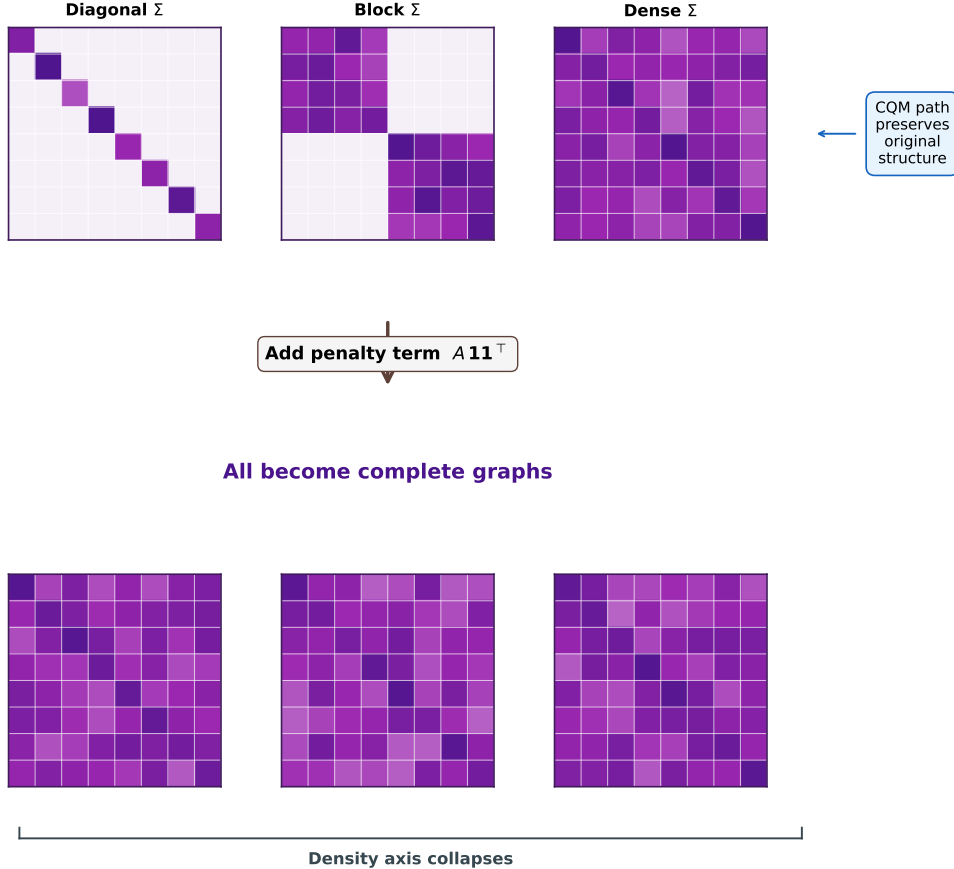


Figure 1: Density-axis collapse under penalty encoding. Three structurally different covariance matrices (diagonal, block, dense) all become complete graphs after adding the cardinality penalty $A \cdot \mathbf{1}\mathbf{1}^\top$. The CQM path preserves the original structure.

Lemma 3 (Embedding-Overhead Growth Drives Chain-Break Frequency). *Under Theorem 1, the mean chain length for the penalty-encoded K_N embedding satisfies $\bar{L}(N) = \Omega(N/d)$ (Corollary 2). Consequently, all else equal — at fixed chain strength J_c , fixed annealing schedule, fixed calibration, and under a per-edge intra-chain disagreement model in which each physical edge in a chain has independent break probability p — the per-chain break probability is a monotone non-decreasing function of $\bar{L}(N)$.*

Empirical manifestation. We confirm density-axis collapse empirically in Section 5.1: chain-break fractions and embedding overheads are nearly identical across diagonal ($\rho \approx 2/N$, decaying with N), block ($\rho \in [0.11, 0.25]$), and dense ($\rho \approx 1.0$) families at each N . Figure 1 illustrates the mechanism schematically; Figure 2 summarises the practical consequences for D-Wave practitioners.

2.6 D-Wave Hardware

We use two D-Wave systems:

- **Advantage_system4.1** (Pegasus topology): 5,760 ideal qubits, degree-15 connectivity. The active qubit count of 5,627 reflects the working graph of Advantage_system4.1 during the experimental campaign (April 2026); embedding statistics in Section 5.1 are computed against this active set.

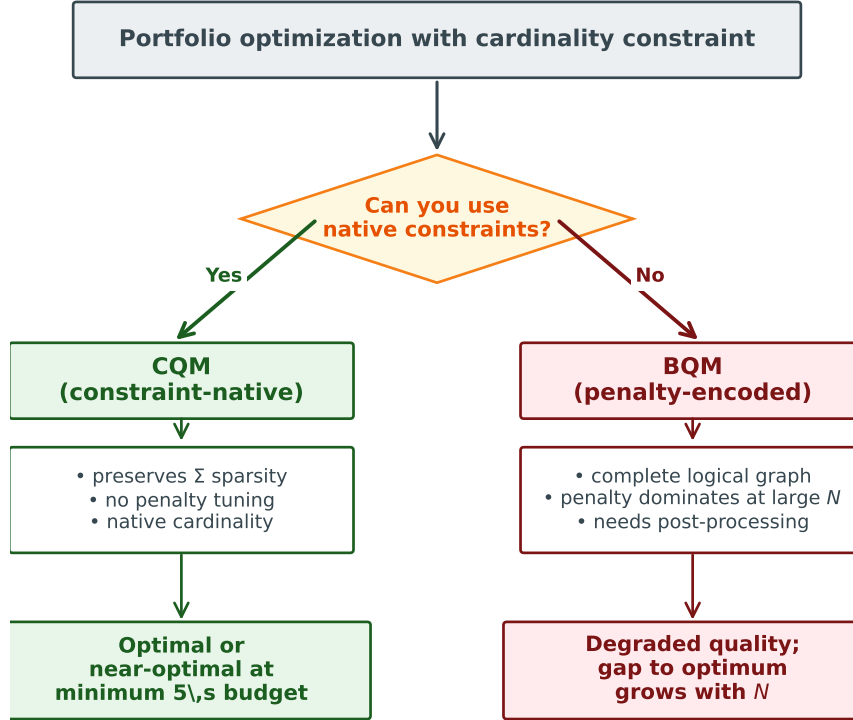


Figure 2: Formulation choice for D-Wave portfolio optimization. The constraint-native CQM path preserves sparsity, requires no penalty tuning, and achieves optimal solutions at the minimum budget. The penalty-encoded BQM path creates a dense graph, degrades with N , and requires budget tuning.

- **Advantage2_system1.13** (Zephyr topology): 4,800 ideal qubits, degree-20 connectivity.²

Direct QPU access requires minor embedding of the logical QUBO graph into the hardware topology. Hybrid solvers (LeapHybridBQMSampler, LeapHybridCQMSampler) accept arbitrary problem structures and manage embedding and QPU allocation internally, with a minimum time limit of approximately 5 seconds [D-Wave Systems, 2025a]. Figure 3 illustrates the hybrid solver architecture.

3 Operational Decomposition Audit Protocol

The findings of this paper depend on a small set of operational metrics that are, in principle, observable from any hybrid quantum-classical solver that exposes per-run resource telemetry. We formalise these metrics as a *decomposition audit protocol*. The protocol is a reusable methodological contribution independent of the specific D-Wave LeapHybrid services audited in Sections 5–6, and is presented as a *candidate minimum reporting standard* for future hybrid quantum-finance benchmarks, for community discussion.

²On 2026-04-10, D-Wave renamed this solver to **Advantage2_system1** and removed qubit 4374 (and its couplers) from the working graph. Embedding records were generated across this study and the companion penalty-encoding paper; we verified that qubit 4374 was not selected by the embedder for any chain, so the rename does not affect any reported result. All experiments here were run before the rename.

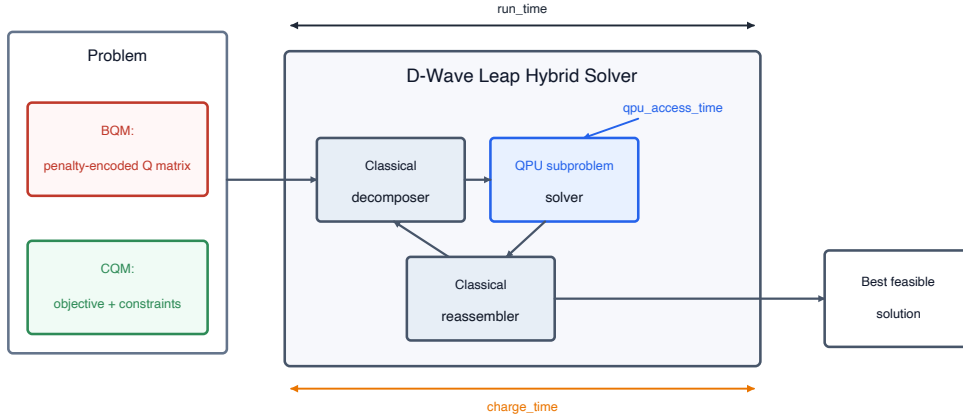


Figure 3: D-Wave hybrid solver architecture. The solver iterates between classical decomposition and QPU subproblem solving. Timing fields (`run_time`, `charge_time`, `qpu_access_time`) are reported separately, allowing analysis of whether the QPU actively contributed to the solution.

3.1 Metrics

Let a hybrid solver run produce a sampleset \mathcal{S} with timing fields t_{run} (total run time), t_{charge} (charged service time), and t_{QPU} (cumulative QPU-access time, summed over all sub-problem QPU calls within the run), each as exposed by the D-Wave Ocean SDK [D-Wave Systems, 2025b]; a final objective value $f_{\mathcal{S}}$; and a best-known classical optimum f^* on the same instance. Let Q_{encoded} be the QUBO matrix actually submitted to the solver, Σ the original covariance matrix (or other cost matrix) before encoding, and $|E(\cdot)|$ the off-diagonal edge count of a matrix (cf. `suppoff` in Theorem 1). We define four metrics.

(M1) QPU wall-clock fraction.

$$r_{\text{QPU}} := \frac{t_{\text{QPU}}}{t_{\text{run}}} \in [0, 1]. \quad (6)$$

r_{QPU} measures the fraction of wall-clock that the service spent on the quantum processor, summed over all sub-problem QPU calls. r_{QPU} is a necessary but not sufficient indicator of quantum contribution: high r_{QPU} does not guarantee that the QPU samples were causally important to the final solution; low r_{QPU} *does* bound the share of wall-clock attributable to quantum sampling from above. In D-Wave Ocean, t_{QPU} is the per-submission cumulative QPU access time, read either as `sampleset.info['qpu_access_time']` or, when nested timing is exposed, as `sampleset.info['timing']['qpu_access_time']`.

(M2) Optimality gap.

$$g_F := \frac{f_{\mathcal{S}} - f^*}{\max(1, |f^*|)}. \quad (7)$$

g_F is the relative objective gap to the best-known classical optimum. The denominator is regularised to handle $|f^*| \rightarrow 0$. A negative g_F indicates the solver outperformed the classical anchor on this instance. g_F is a *solver-side* metric; portfolio-level financial metrics (Sharpe, deflated Sharpe) are computed on realised return time series with their own denominators (Section 5.6) and are not interchangeable with g_F .

(M3) Encoded-graph density amplification. Let $E_{\text{enc}} := |E(Q_{\text{encoded}})|$ and $E_{\text{orig}} := |E(\Sigma)|$. Define

$$d_{\text{amp}} := \begin{cases} E_{\text{enc}}/E_{\text{orig}} & \text{if } E_{\text{orig}} > 0, \\ \infty & \text{if } E_{\text{orig}} = 0 \text{ and } E_{\text{enc}} > 0, \\ 1 & \text{if } E_{\text{enc}} = E_{\text{orig}} = 0. \end{cases} \quad (8)$$

By Theorem 1, penalty-encoded paths satisfy $d_{\text{amp}} = \binom{N}{2}/E_{\text{orig}}$ when $E_{\text{orig}} > 0$, and $d_{\text{amp}} = \infty$ when Σ is diagonal; constraint-native CQM paths satisfy $d_{\text{amp}} = 1$ by the CQM support-preservation remark after Theorem 1. We recommend reporting raw E_{enc} and E_{orig} alongside the ratio to keep the diagonal- Σ case visible.

(M4) Service-variance.

$$v_{\text{service}}(N, \rho, B) := \text{Var}(f_S \mid N, \rho, B, \text{seed} \in \mathcal{R}), \quad (9)$$

the variance of the solver’s final objective at fixed problem dimension N , density family ρ , and wall-clock budget B , over a set \mathcal{R} of repeated calls with $|\mathcal{R}| \geq 10$. $v_{\text{service}} = 0$ indicates a deterministic service on the tested class. The $|\mathcal{R}| = 1$ case is excluded because $v_{\text{service}} = 0$ would be tautological.

3.2 Audit procedure

We propose that any hybrid quantum-classical benchmark report the following items.

- (P1) **All three timing fields** per run: t_{run} , t_{charge} , t_{QPU} . Do not report only t_{QPU} .
- (P2) **r_{QPU} distribution** per (N, ρ) cell, with at least mean and inter-quartile range; not a point estimate.
- (P3) **Optimality gap** g_F computed against the strongest available classical optimum at *matched wall-clock*. “Matched wall-clock” means the classical solver is allotted the same t_{run} as the hybrid service; if it converges or proves optimality earlier, the earlier wall-clock is reported alongside. Report the classical solver name, version, and wall-clock used.
- (P4) **Encoded-graph density amplification** d_{amp} for every formulation variant. Report raw E_{enc} and E_{orig} alongside the ratio. Explicitly contrast penalty-encoded and constraint-native paths.
- (P5) **Feasibility rate before and after post-processing repair**. For penalty-encoded paths, separate the raw-sample feasibility rate from the post-projection feasibility rate.
- (P6) **Service-variance** v_{service} over ≥ 10 repeated calls per cell. Distinguishes deterministic service runs from stochastic ones.
- (P7) **Solver identity and campaign window**. For D-Wave Leap, record the sampler’s solver identity at submission time (`sampler.solver.identity`, or `sampler.solver.name` as a fallback) plus the submission `problem_id`. The legacy `sampleset.info['solver']` field is unreliable across SDK versions and should not be used as the canonical version source. Also record the start and end dates of the run campaign.

3.3 Applicability

The protocol applies directly to hybrid services that expose the three timing fields above as first-class telemetry — specifically, D-Wave Leap hybrid solvers (LeapHybridCQMSampler and LeapHybridBQMSampler), which return `run_time`, `charge_time`, and `qpu_access_time` on every submission. Adapting the protocol to other hybrid services (AWS Braket Hybrid Jobs, Qiskit Runtime Estimator-based hybrid optimisers) is possible but requires platform-specific instrumentation: those services expose only partial or aggregate metrics (e.g., quantum-task counts and latencies, or `quantum_seconds`) rather than a direct $(t_{\text{run}}, t_{\text{charge}}, t_{\text{QPU}})$ tuple. We do not validate the protocol on these alternative services in the present paper.

3.4 Reference implementation

A reference implementation of the four metrics, ingesting a saved hybrid sampleset record and emitting a structured JSON audit report, accompanies this paper at the URL given in the Data-and-Code-Availability statement. The same repository contains the analysis scripts that produced every empirical result reported in Sections 5–6, including the QPU-replacement ablation (Section 5.9).

3.5 Interpretive limits

The protocol has several interpretive limits, which we state explicitly.

r_{QPU} is wall-clock, not causal. A run with $r_{\text{QPU}} = 0.5$ may still be classical-dominated if the QPU samples are ignored by the reassembler; a run with $r_{\text{QPU}} = 0.007$ may still have a QPU contribution that is structurally necessary if the classical decomposer’s logic is tuned to QPU-shaped sub-problems. The protocol does not resolve this ambiguity. Resolving it requires a *QPU-replacement ablation* in which the QPU sub-solver is replaced by an equivalent classical sub-solver at matched per-call budget — an experiment we approximate in Section 5.9 with a CPU-only counterfactual.

Solver-version drift. Commercial hybrid services version their internal solver behind a stable user-facing interface; timing distributions and qualitative behaviour can change between solver-version updates. The protocol therefore requires (P7) the explicit recording of the solver identity and campaign window, and benchmark results should not be extrapolated across version boundaries without re-running the audit.

Working-graph and calibration drift. For direct-QPU paths, the working graph (active qubits and couplers) and the per-qubit calibration drift across calibration cycles. Runs within a single calibration cycle are comparable; runs across cycles are not, unless the calibration is explicitly recorded and accounted for.

Timing-field granularity and client/service wall-clock. t_{run} as reported by the service is the service-side wall-clock; the client-side wall-clock (including network round-trips and queue waits) is generally larger and depends on operational conditions. r_{QPU} uses the service-side denominator and therefore overstates the QPU’s share of the user-observed latency.

No latency or queue-time metrics. In production deployment, queue depth, batch latency, and service-level objectives matter as much as the four metrics above. The protocol is a measurement framework for solver behaviour, not a service-level-agreement framework.

4 Experimental Setup

4.1 Synthetic Controlled Instances

We generate controlled benchmark instances across three covariance-density families:

- **Diagonal:** near-banded covariance with light nearest-neighbour off-diagonal noise ($\epsilon = 0.02$); per-instance density decays as $\rho \approx 2/N$, from ≈ 0.20 at $N=10$ to below 0.01 at $N \geq 200$.
- **Block-diagonal:** equicorrelated blocks with zero cross-block interaction; per-instance density $\rho \in [0.11, 0.25]$ depending on N and block structure.
- **Dense:** full covariance matrices from Wishart draws ($\rho \approx 1.0$).

The structural results in Section 2.5 depend only on the support pattern of the encoded QUBO and are invariant to any positive linear rescaling of $\boldsymbol{\mu}$. The empirical CQM-vs-BQM quality comparison in Section 5.2 is, by contrast, scale-dependent: at the chosen parameterization the penalty term $A \cdot \mathbf{1}\mathbf{1}^\top$ with $A = 4.0$ dominates the linear return contribution at large N , driving the observed BQM degradation. Synthetic instances use $\boldsymbol{\mu} \sim \mathcal{N}(0.05, 0.02)$ as unitless signal coefficients scaled for numerical stability; per-variable variance scales are drawn independently from $\mathcal{U}(0.02, 0.08)$. Financial metrics (Sharpe, deflated Sharpe ratio, etc.) are reported only on the realized Fama–French 49 industry portfolio data in Section 5.6, not on the synthetic instances. All covariance matrices are symmetric positive definite by construction. Each configuration is run with three random seeds. Cardinality is set to $K = \lfloor 0.3N \rfloor$ and risk aversion to $\lambda = 0.5$.

4.2 Real Equity Data

We use the Fama–French 49 industry daily return portfolios [French, 2026], constructing rolling estimation windows of 252 trading days with monthly rebalancing. Five evenly spaced windows are selected. Industry subsets of $N \in \{10, 20, 30\}$ are formed by selecting the industries with the largest absolute expected-return magnitude.

4.3 Solver Configurations

Direct QPU. Forward annealing on both Pegasus and Zephyr with 1000 reads, annealing time $20 \mu\text{s}$, chain strengths $\{0.5, 1.0, 2.0\}$, and multi-seed embedding search (5 seeds, 20 tries per seed). All direct-QPU experiments use the default gauge setting (single-gauge sampling with no spin-reversal transforms); multi-gauge robustness checks are deferred to future work. Post-processing projects each sample to exact- K feasibility using the greedy projection of Lozano [2026].

Hybrid BQM. LeapHybridBQMSampler with the penalty-encoded QUBO (3), $A = 4.0$. The penalty value is consistent with the calibration study of Lozano [2026]; we verify robustness to $A \in \{2.0, 4.0, 8.0\}$ in Appendix A. Post-processing projects to exact- K .

Hybrid CQM. LeapHybridCQMSampler with the constraint-native formulation (4). Cardinality is enforced natively; the solver returns feasible solutions directly.

Gurobi MIQP. The cardinality-constrained MVT problem (2) is solved as a native mixed-integer quadratic program using Gurobi 13.0 (Gurobi Optimization, LLC) with a 300-second time limit. Gurobi proves optimality on all tested instances at $N \leq 200$ (62 of 63 attempted runs; one $N=200$ run reached the time limit); at $N \geq 400$ the academic license does not support the model size. Gurobi serves as the gold-standard reference where optimality is proven.

Simulated annealing. D-Wave’s `neal` simulated-annealing sampler (1000 reads, 1000 sweeps) applied to the penalty-encoded BQM (3). Solutions are projected to exact- K with the same post-processing as the QPU path.

4.4 Benchmark Axes

1. **Problem size N :** $\{10, 20, 30, 50, 80\}$ for direct QPU; $\{10, 20, 30, 50, 80, 120, 200, 400, 640\}$ for hybrid and classical solvers.
2. **Covariance density:** diagonal, block, dense.
3. **Wall-clock budget:** $\{5, 30, 60, 180, 300\}$ seconds for hybrid budget sweep (Section 5.7).

5 Results

5.1 Direct QPU: Chain-Break Fractions and Embedding Overhead

Table 1 reports the mean chain-break fraction and embedding overhead for direct QPU sampling of the penalty-encoded QUBO, and Figure 4 visualizes these trends split by hardware topology (Pegasus vs Zephyr). Chain-break fractions increase monotonically with N , reaching 0.937 ± 0.016 at $N = 80$. The embedding overhead grows from $1.6\times$ at $N = 10$ to $9.4\times$ at $N = 80$. These trends are consistent with the cross-generation chain-break and embedding-overhead measurements reported by Pelofske [2025] for combinatorial benchmark problems on Pegasus and Zephyr.

Table 1: Direct QPU embedding statistics (mean \pm std over all families, seeds, topologies, and chain strengths; 270 runs, all embedded successfully). Chain-break fractions and embedding overheads are nearly identical across density families at each N , confirming the density-axis collapse of Section 2.5.

N	K	Chain-break frac.	Phys. qubits	Overhead
10	3	0.543 ± 0.058	16	$1.6\times$
20	6	0.756 ± 0.034	51	$2.5\times$
30	9	0.820 ± 0.019	107	$3.6\times$
50	15	0.894 ± 0.023	298	$6.0\times$
80	24	0.937 ± 0.016	750	$9.4\times$

At chain-break fractions above 0.9, the majority of QPU samples contain broken chains, meaning the decoded solutions reflect the post-processing repair heuristic more than the annealing dynamics. This is a direct consequence of the $A \cdot \mathbf{11}^\top$ penalty term, which forces the complete-graph embedding regardless of the original Σ density. Figure 5 confirms this empirically: chain-break fractions are nearly identical across diagonal, block, and dense families at each N , on both Pegasus and Zephyr.

Per-chain-strength refinement. Table 1 averages over chain strengths $J_c \in \{0.5, 1.0, 2.0\}$. Because all three sit at or below the penalty magnitude $|J_{\max}| = A = 4.0$, the averaged report risks blurring the distinction between guaranteed-broken and working regimes. Table 2 splits the same data by chain strength. The qualitative finding is robust: at the strongest tested $J_c = 2.0$, CBF is already ≈ 0.81 at $N = 30$, exceeds 0.88 by $N = 50$, and reaches 0.92 at $N = 80$. The difference between $J_c = 0.5$ and $J_c = 2.0$ is small (~ 0.03 in CBF at $N = 80$), showing that the chain-break problem on the penalty-encoded K_N embedding is structural — driven by chain length growth on the fully-connected logical graph (Lemma 3) — rather than by chain-strength tuning.

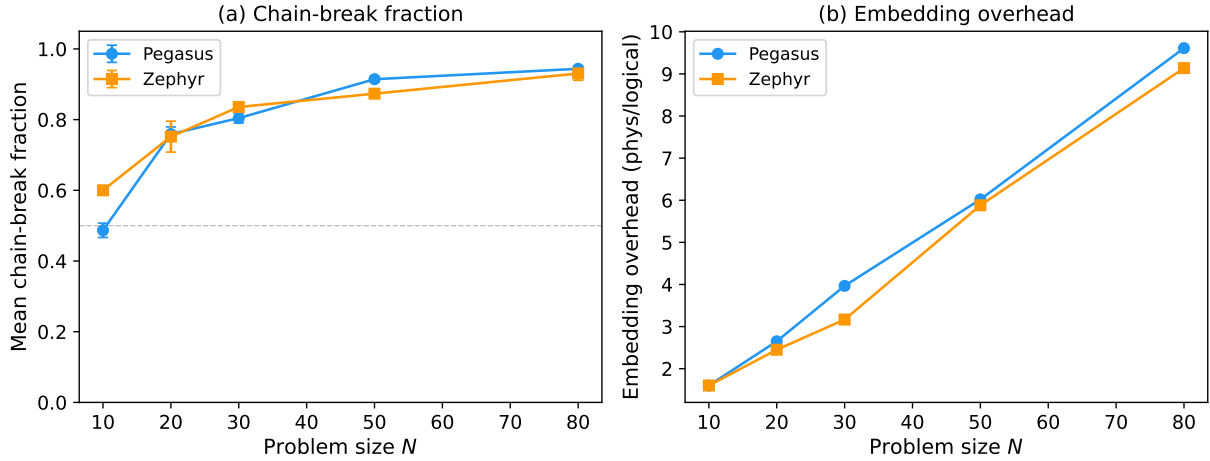


Figure 4: (a) Mean chain-break fraction and (b) embedding overhead (physical / logical qubits) vs problem size for direct QPU on penalty-encoded QUBOs, split by hardware topology.

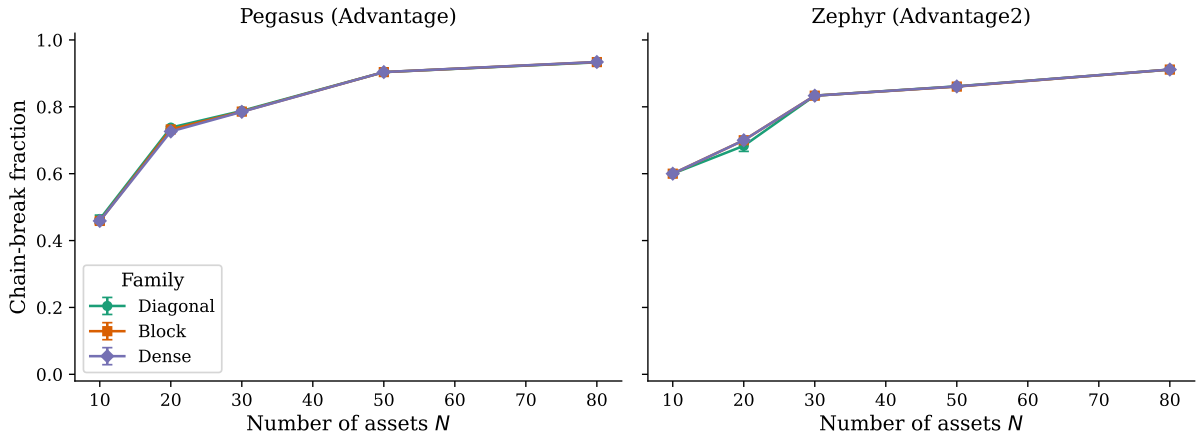


Figure 5: Chain-break fraction vs N split by covariance-density family (diagonal, block, dense), on Pegasus (left) and Zephyr (right). The three curves nearly overlap at each N , confirming that penalty encoding collapses the density axis.

5.2 Hybrid CQM vs BQM: Formulation Comparison

Table 3 compares the mean objective values achieved by hybrid BQM and CQM across problem sizes. All values are evaluated on the original constrained objective (2): BQM solutions are projected to exact- K before evaluation.

At $N \geq 200$, the BQM objective becomes positive: the penalty term dominates the economic signal, and the hybrid solver allocates its budget to penalty satisfaction rather than objective optimization. Under the exact- K cardinality constraint, a positive objective value indicates a portfolio whose risk-adjusted cost exceeds its expected return. The CQM formulation avoids this failure mode because the cardinality constraint is handled natively.

Figure 6 visualizes the solver comparison including classical baselines.

5.3 Gap to Gurobi Optimal

Table 4 and Figure 7 report the relative gap to Gurobi’s proven optimum, defined as $(f_{\text{solver}} - f^*)/|f^*|$ where f^* is the Gurobi-optimal objective. CQM matches the proven optimum exactly (gap = 0) on all 54 head-to-head instances at $N \leq 120$ (6 sizes \times 9 instances per N , all of which Gurobi proves to optimality). BQM and SA, both operating on the penalty-encoded formulation,

Table 2: Direct-QPU chain-break fraction split by chain strength J_c (mean \pm sample std over density families, seeds, and topologies). At $J_c \leq 1.0$ the chain strength sits at or below the penalty magnitude $|J_{\max}| = A = 4.0$, so chain breaks are guaranteed by construction; only $J_c = 2.0$ is plausibly in a working regime, and even $J_c = 2.0$ is below the rule-of-thumb $1.5|J_{\max}| = 6.0$. This per-strength split refines the chain-strength-averaged summary in Table 1.

N	J_c	runs	CBF mean \pm std	Phys. overhead
10	0.5	18	0.550 ± 0.051	$1.6\times$
10	1.0	18	0.550 ± 0.051	$1.6\times$
10	2.0	18	0.530 ± 0.073	$1.6\times$
20	0.5	18	0.785 ± 0.014	$2.5\times$
20	1.0	18	0.768 ± 0.006	$2.5\times$
20	2.0	18	0.713 ± 0.023	$2.5\times$
30	0.5	18	0.828 ± 0.012	$3.6\times$
30	1.0	18	0.822 ± 0.013	$3.6\times$
30	2.0	18	0.810 ± 0.024	$3.6\times$
50	0.5	18	0.905 ± 0.018	$6.0\times$
50	1.0	18	0.895 ± 0.024	$6.0\times$
50	2.0	18	0.882 ± 0.022	$6.0\times$
80	0.5	18	0.955 ± 0.002	$9.4\times$
80	1.0	18	0.934 ± 0.011	$9.4\times$
80	2.0	18	0.922 ± 0.011	$9.4\times$

show monotonically increasing gaps.

5.4 Classical Baselines: Gurobi MIQP and Simulated Annealing

Gurobi MIQP solves all tested instances to proven optimality at $N \leq 200$ (62 of 63 runs; one $N = 200$ run reached the time limit). At $N \geq 400$, the free academic license does not support the model size. The neal simulated-annealing heuristic, which operates on the same penalty-encoded BQM as the hybrid BQM solver, exhibits a similar degradation pattern: objective quality deteriorates at large N where the penalty term dominates. This confirms that the BQM degradation is a formulation effect, not a solver-specific artifact.

5.5 Full Hybrid Timing Breakdown

Table 5 reports the three timing fields the D-Wave hybrid SDK exposes per submission — t_{run} , t_{charge} , and t_{QPU} — as means over the 9 instances per (N, solver) cell of the synthetic-hybrid campaign (162 runs total). The QPU wall-clock fraction $r_{\text{QPU}} = t_{\text{QPU}}/t_{\text{run}}$ (Section 3.1) is included as the rightmost column.

Three observations:

- For LeapHybridCQM, t_{QPU} is approximately constant in N (~ 34 ms across all sizes from $N=10$ to $N=640$), while t_{run} and t_{charge} stay close to the service’s 5 s minimum. The result is $r_{\text{QPU}} \in [0.67\%, 0.77\%]$ across the entire N range, with no monotonic trend; this is the $\approx 0.7\%$ headline number.
- For LeapHybridBQM, t_{QPU} is larger ($\sim 147\text{--}187$ ms) and varies more across N , peaking near $N = 200$; r_{QPU} is in the range $[2.95\%, 3.75\%]$, roughly $4\times$ the CQM value.

Table 3: Hybrid CQM vs BQM: mean objective value by N (averaged over 3 density families \times 3 seeds = 9 instances per N ; 162 runs total). Lower is better. “CQM strict wins” counts instances with $f_{\text{CQM}} < f_{\text{BQM}} - \varepsilon$, $\varepsilon = 10^{-6}$; “ties” counts $|f_{\text{CQM}} - f_{\text{BQM}}| \leq \varepsilon$. A paired Wilcoxon signed-rank test on per-instance objectives rejects $H_0 : f_{\text{CQM}} = f_{\text{BQM}}$ at every $N \geq 20$ ($p < 0.05$; $p = 0.031$ at $N = 20$, $p = 0.002$ at $N \geq 30$); at $N=10$ all nine pairs are ties.

N	BQM objective	CQM objective	CQM strict wins	Ties
10	-0.139	-0.139	0/9	9
20	-0.310	-0.315	5/9	4
30	-0.417	-0.455	9/9	0
50	-0.540	-0.654	9/9	0
80	-0.622	-0.955	9/9	0
120	-0.628	-1.247	9/9	0
200	+0.024	-1.525	9/9	0
400	+4.480	+0.040	9/9	0
640	+16.452	+6.229	9/9	0

Table 4: Relative gap to Gurobi optimal (mean \pm sample std, ddof=1, over 9 instances per N). CQM achieves zero gap at every N . BQM and SA gaps grow with N as penalty dilution intensifies. The large std at $N=120$ is dominated by a single outlier instance; median values are within a factor of two of the means in every cell.

N	CQM gap	BQM gap	SA gap
10	0.000	0.000	0.000
20	0.000	0.016 ± 0.020	0.065 ± 0.044
30	0.000	0.084 ± 0.026	0.146 ± 0.023
50	0.000	0.184 ± 0.058	0.250 ± 0.089
80	0.000	0.622 ± 0.666	0.728 ± 0.687
120	0.000	3.136 ± 5.125	3.985 ± 6.638

- In both solvers, $t_{\text{run}} \approx t_{\text{charge}}$ (within $\sim 3\%$), so the choice of denominator does not materially change the reported QPU fraction.

The fraction of runs where the QPU actively contributed (`qpu_access_time` $>$ 0) is 80/81 for hybrid BQM and 79/81 for hybrid CQM; in the budget sweep (Section 5.7) the QPU contributed in 74/78 runs across both solvers.

The constancy of t_{QPU} in N on the CQM path is consistent with a classical decomposer that breaks any instance into bounded-size sub-problems before dispatching them to the QPU; the scale-up cost is paid by the classical decomposer, not by the QPU. The interpretive limits of Section 3.5 apply: r_{QPU} bounds the *wall-clock* share, not the causal contribution. Section 5.8 and Section 5.9 bound the causal share empirically.

5.6 Direct QPU on Real Equity Data

We confirm the synthetic findings on Fama–French 49 industry data as a directional sanity check (90 runs). Chain-break fractions follow the same pattern as the synthetic instances: 0.483 at $N = 10$, 0.759 at $N = 20$, and 0.802 at $N = 30$ (Pegasus means). All 90 embeddings succeeded; the constraint is solution quality, not embedding feasibility. Figure 8 shows the chain-break trend on real data.

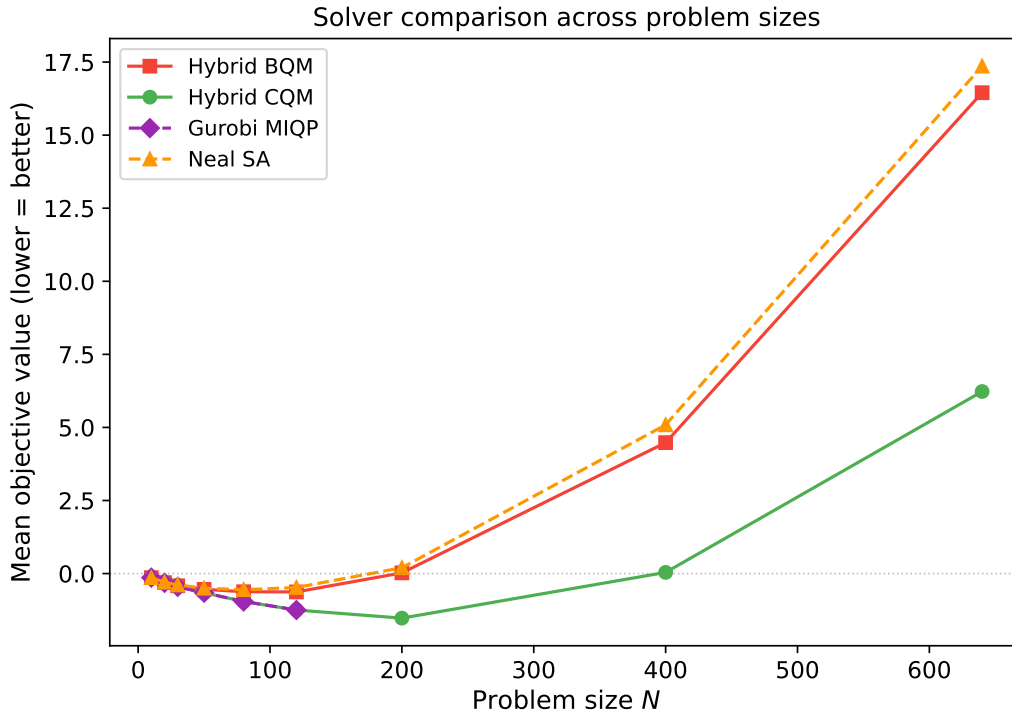


Figure 6: Mean objective value vs problem size across solver families (averaged over 3 density families \times 3 seeds). Gurobi MIQP (dashed purple) provides provably optimal solutions. Hybrid CQM (green) tracks Gurobi closely. Hybrid BQM (red) and Neal SA (orange) both operate on the penalty-encoded QUBO and diverge at large N .

5.7 Budget Sweep: Does More Time Help?

Table 6 reports hybrid objective values across wall-clock budgets from 5 to 300 seconds, and Figure 9 visualizes the corresponding budget response curves. The budget sweep uses $N \in \{50, 100, 200, 400\}$ (differing from the main N -sweep grid to include mid-range sizes relevant for budget sensitivity).

Stochastic validation. To verify that the budget-saturation finding is not an artifact of single-shot runs, we repeat the hybrid CQM and BQM solves 10 times each at $N \in \{50, 100, 200\}$, both density families, and budgets $\{5, 300\}$ s (228 runs total; the ($N=50$, dense, 300s) cell completed four repetitions within the campaign’s wall-clock budget, the remaining cells reached the planned ten). Hybrid CQM produced bitwise-identical objective values (zero variance to floating-point precision) across all available repetitions at every tested (N, ρ, B) combination, at both 5s and 300s — verified at the cell level against the saved JSONL records. BQM shows measurable stochastic variance (std 0.01–0.12) and improves with budget, but its best run at 300s never reaches the CQM objective at 5s on any tested instance. Figure 10 visualizes this contrast.

5.8 QPU-Dwell vs Solution-Quality Correlation

The QPU wall-clock fraction r_{QPU} bounds the time share attributable to the quantum processor but cannot, by itself, bound the QPU’s causal contribution to solution quality. We bound the causal contribution in two complementary ways: within-cell correlation between QPU dwell time and final objective (this subsection); and a CPU-only QPU-replacement ablation (Section 5.9).

Within-cell analysis. Within each (N, ρ, B) cell, repeated hybrid CQM calls produce bitwise-identical objective values (Section 5.7), so within-cell correlation analysis is only defined on

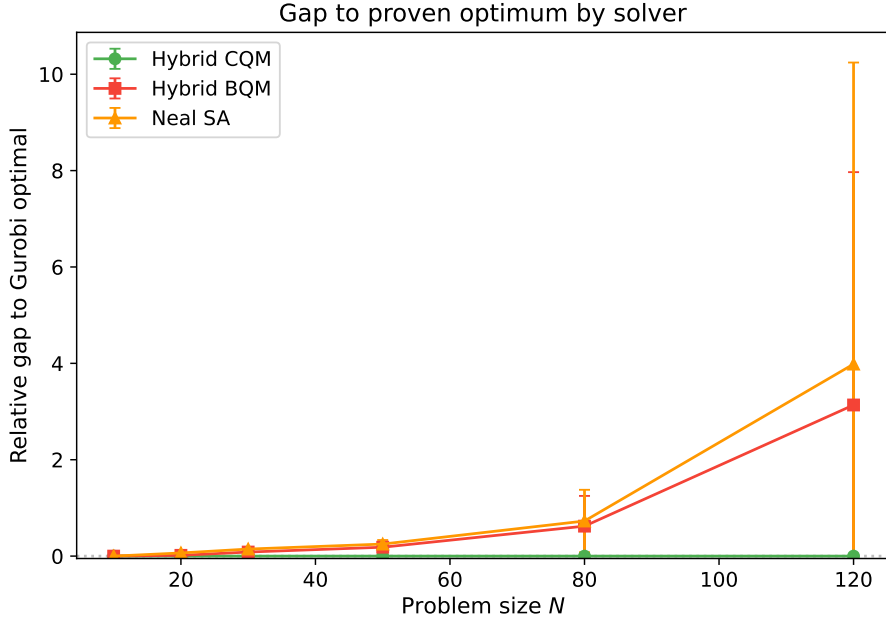


Figure 7: Relative gap to Gurobi optimal vs N . CQM (green) is indistinguishable from the optimal baseline; BQM (red) and SA (orange) diverge as penalty dilution intensifies.

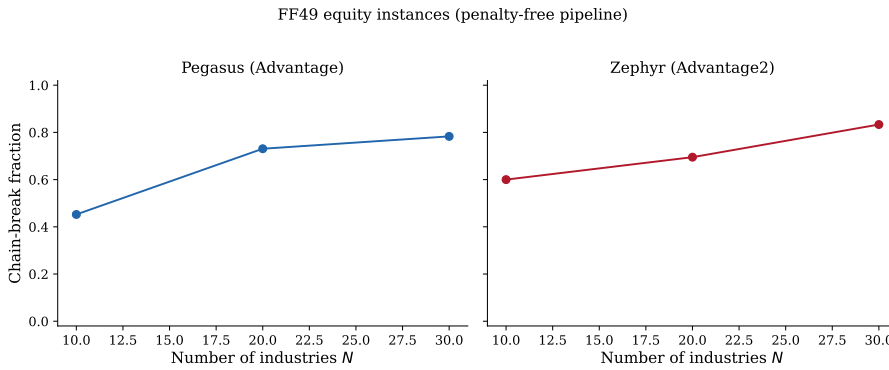


Figure 8: Direct QPU on real Fama–French 49 equity data: chain-break fraction vs N on Pegasus and Zephyr, confirming the synthetic-data pattern on real financial covariance matrices.

hybrid BQM cells where service-internal randomness produces measurable objective variance. On 11 such BQM cells (extracted from the repeated-hybrid campaign at $N \in \{50, 100, 200\}$, {block, dense}, {5, 300} s), we compute Spearman ρ between `hybrid_qpu_access_time` and `objective_value`, with 95% bootstrap confidence intervals (2,000 resamples).

The result is mostly null. Nine of 11 cells have CIs that straddle zero. One cell ($N = 100$, block, 5 s) shows significant negative $\rho = -0.78$ (CI $[-1.00, -0.17]$) — more QPU dwell associated with better objective; one cell ($N = 200$, dense, 5 s) shows significant positive $\rho = +0.81$ (CI $[+0.16, +1.00]$) — more QPU dwell associated with worse objective. The two significant cells cancel qualitatively, and the median $|\rho|$ across all 11 cells is 0.27 with high CI overlap. At the within-cell level, hybrid BQM service randomness does not produce a consistent QPU-dwell-vs-quality relationship.

Cross-cell analysis at fixed (solver, N). We also compute Spearman ρ across the different (ρ, B) cells at fixed (solver, N) in the budget sweep, where 10 distinct cells per (solver, N) vary in family and budget. Of 8 cross-cell buckets analysed, 2 have CIs strictly below zero (more QPU

Table 5: Full timing breakdown per (N, solver) cell on the synthetic-hybrid runs (mean over 9 instances per cell: 3 density families \times 3 seeds; 162 runs total). All timing fields in seconds. r_{QPU} is the within-cell mean wall-clock fraction $t_{\text{QPU}}/t_{\text{run}}$.

N	Solver	t_{run} (s)	t_{charge} (s)	t_{QPU} (s)	r_{QPU} (%)
10	hybrid-bqm	4.987	4.987	0.1469	2.95
20	hybrid-bqm	4.987	4.987	0.1516	3.04
30	hybrid-bqm	4.991	4.991	0.1564	3.13
50	hybrid-bqm	4.989	4.989	0.1626	3.26
80	hybrid-bqm	4.994	4.994	0.1855	3.71
120	hybrid-bqm	4.996	4.996	0.1671	3.34
200	hybrid-bqm	4.991	4.991	0.1873	3.75
400	hybrid-bqm	4.994	4.994	0.1553	3.11
640	hybrid-bqm	4.987	4.987	0.1556	3.12
10	hybrid-cqm	4.613	4.569	0.0347	0.76
20	hybrid-cqm	4.514	4.488	0.0347	0.77
30	hybrid-cqm	4.842	4.745	0.0347	0.72
50	hybrid-cqm	4.582	4.564	0.0309	0.68
80	hybrid-cqm	4.683	4.641	0.0309	0.67
120	hybrid-cqm	4.506	4.488	0.0347	0.77
200	hybrid-cqm	4.927	4.813	0.0347	0.71
400	hybrid-cqm	4.937	4.822	0.0347	0.71
640	hybrid-cqm	4.973	4.826	0.0348	0.70

dwell \leftrightarrow better objective), 0 have CIs strictly above zero, and 6 straddle zero. The two significant negative cases (BQM $N = 400$ and CQM $N = 50$) are consistent with the classical decomposer allocating more QPU time to harder sub-problems within the same N — a hardness-correlated allocation pattern rather than a causal contribution from the QPU samples themselves.

Taken together, the dwell-vs-quality analysis is consistent with the $\approx 0.7\%$ wall-clock fraction being non-causal at the within-cell level; it does not, however, *prove* non-causality. The ablation in Section 5.9 addresses that question directly.

5.9 QPU-Replacement Ablation at Matched Wall-Clock

To bound the share of hybrid CQM solution quality that quantum sampling could be contributing on this problem class, we performed a CPU-only counterfactual: on 24 instances ($N \in \{50, 80, 120, 200\}$, {block, dense}, three seeds each), we ran the `TabuSampler` from D-Wave’s classical-samplers package on the same penalty-encoded BQM that `LeapHybridBQM` consumes, at a matched wall-clock budget of 5 s per instance (matching the hybrid service’s 5 s minimum). The ablation grid starts at $N = 50$ because hybrid CQM and BQM tie at $N = 10$ on every seed (Table 3) and the head-to-head gap is small through $N = 30$, leaving little ablation signal at the smaller sizes. Results were projected to exact- K feasibility using the same greedy projector [Lozano, 2026] as the direct-QPU path; the final mean-variance-turnover objective was then evaluated.

Table 7 reports the resulting Tabu objectives alongside the saved hybrid CQM, hybrid BQM, and Gurobi-optimal objectives for the same $(N, \text{family}, \text{seed})$ instances.

Aggregated across all 24 instances:

- Mean(Tabu – Hybrid CQM) = +0.00107; max |Tabu – CQM| = 0.00798. 18 of 24 instances match to within 0.0005.

Table 6: Hybrid objective value by wall-clock budget (dense family; block family shows the same pattern, with two hybrid BQM block-family cells at $N=400$ at 180s and 300s not completed within the campaign’s wall-clock budget — the corresponding CQM cells did complete). On the tested instances, CQM returns bitwise-identical objective values at all budgets; BQM improves with time but does not reach the CQM objective at any budget.

N	Solver	5 s	30 s	60 s	180 s	300 s
50	BQM	-0.633	-0.669	-0.709	-0.696	-0.734
50	CQM	-0.799	-0.799	-0.799	-0.799	-0.799
100	BQM	-1.309	-1.367	-1.593	-1.792	-1.695
100	CQM	-1.839	-1.839	-1.839	-1.839	-1.839
200	BQM	-2.420	-2.460	-2.423	-2.446	-2.480
200	CQM	-3.598	-3.598	-3.598	-3.598	-3.598
400	BQM	-4.426	-4.921	-5.080	-5.740	-5.899
400	CQM	-7.454	-7.454	-7.454	-7.454	-7.454

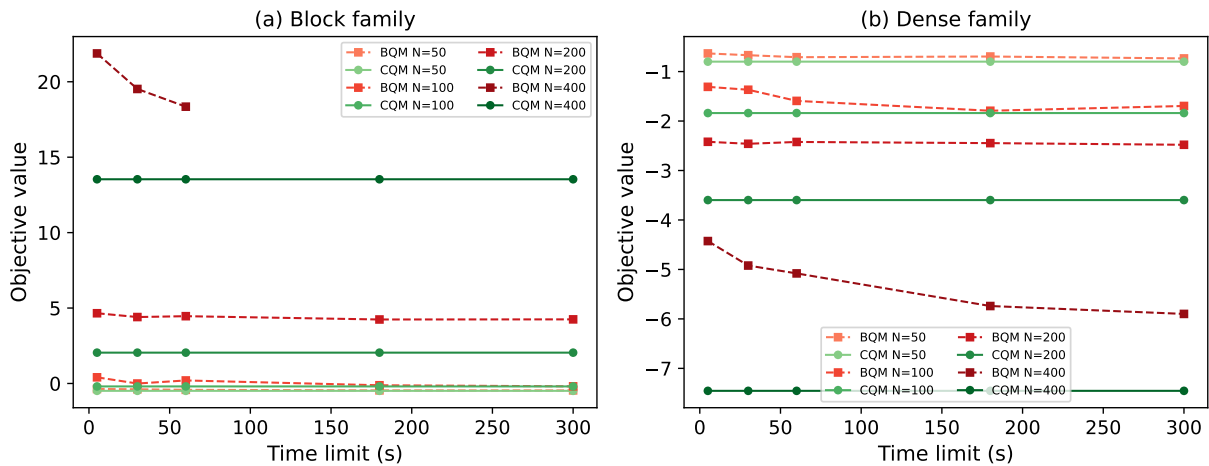


Figure 9: Budget response curves for hybrid BQM (dashed) and CQM (solid) across problem sizes. CQM lines are flat; BQM lines improve with budget but remain above CQM at all tested budgets.

- Mean(Tabu – Gurobi) = +0.00111; max |Tabu – Gurobi| = 0.00798. 17 of 23 head-to-head-to-Gurobi cases match to within 0.0005.
- Mean(Tabu – Hybrid BQM) = -0.76644. Tabu substantially outperforms LeapHybrid-BQM on the same penalty-encoded inputs, so the hybrid-BQM degradation reflects the interaction of the BQM encoding with the LeapHybridBQM pipeline, not quantum sampling alone.

Interpretation. At matched 5 s wall-clock, a strong classical heuristic on the penalty-encoded BQM produces objectives essentially indistinguishable from those produced by the hybrid CQM service on the same instances (median absolute Tabu – CQM gap < 0.001 across 24 cells, in objective units where the cell’s natural scale runs from ≈ 0.5 to ≈ 4). Because the penalty-encoded BQM and the constraint-native CQM encode the same cardinality-constrained MVT problem, recovering Gurobi-optimal (or CQM-matching) objectives on the BQM is equivalent to recovering the same portfolio \mathbf{z}^* that the CQM path recovers; the encoding differs, but the feasible set and the optimal solution do not. This is *not* a LeapHybridCQM internal ablation:

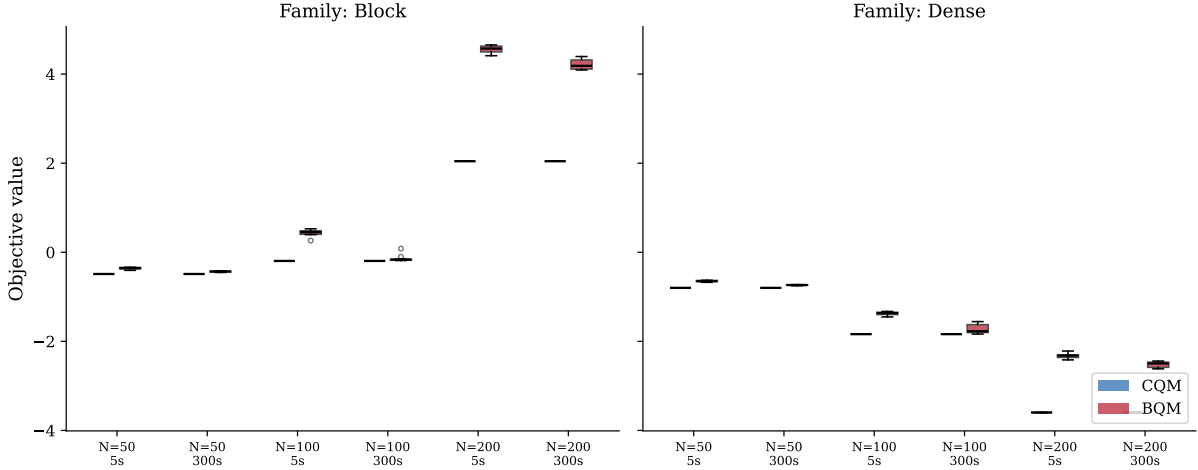


Figure 10: Stochastic validation: box plots of objective values across 10 repeated runs for CQM (green, flat lines = zero variance) and BQM (red, visible spread) at budgets of 5 s and 300 s, split by density family.

Table 7: QPU-replacement ablation: `TabuSampler` at matched 5 s wall-clock on the penalty-encoded BQM, compared to the saved hybrid and Gurobi objectives on the same (N , family, seed) instances. Means over 3 seeds per (N , family) cell; lower is better. The rightmost column is the Tabu-CQM delta (positive means Tabu worse than hybrid CQM).

N	Family	Tabu	Hybrid CQM	Hybrid BQM	Gurobi*	Tabu - CQM
50	block	-0.4731	-0.4746	-0.3555	-0.4746	+0.0015
50	dense	-0.7986	-0.7986	-0.6736	-0.7986	+0.0000
80	block	-0.3099	-0.3136	+0.0691	-0.3136	+0.0037
80	dense	-1.3721	-1.3721	-1.0242	-1.3721	+0.0000
120	block	+0.0099	+0.0075	+0.8249	+0.0075	+0.0024
120	dense	-2.0716	-2.0716	-1.4535	-2.0716	+0.0000
200	block	+1.9404	+1.9395	+4.3947	+1.9395	+0.0009
200	dense	-3.5833	-3.5833	-2.3086	-3.6225 [†]	+0.0000

* Gurobi proves optimality on all reported cells except ($N = 200$, dense, seed = 1), marked [†], which hit `status_9` in the academic-license run.

the hybrid CQM pipeline consumes a different problem encoding and we do not have access to its proprietary internals. What the result *does* show is that the objective levels reached by hybrid CQM on this problem class are reproducible by a classical heuristic at the same wall-clock budget on the penalty-encoded variant; combined with the $\approx 0.7\%$ measured QPU wall-clock fraction (Section 5.5), this is consistent with a very small causal quantum-sampling contribution to the share of solution quality that any quantum contribution *could* be providing on this problem class.

Tabu’s substantial improvement over LeapHybridBQM (mean ~ 0.77 in absolute objective) is consistent with the LeapHybridBQM pipeline being limited by the interaction between its penalty-encoded input and its specific decomposition policy, rather than by classical-heuristic capability or quantum sampling. By contrast the constraint-native LeapHybridCQM pipeline, which avoids the penalty term $A \cdot \mathbf{11}^\top$ that fully connects the encoded logical graph (Theorem 1), reaches the same objective levels as a strong classical heuristic alone.

5.10 Descriptive FF-49 Financial Overlay

The synthetic-instance results (Sections 5.1–5.7) measure solver behaviour on controlled QUBOs; they do not directly answer the question a quantitative portfolio manager will ask — whether the resulting portfolios are competitive against simple financial baselines. We complement the solver-side analysis with an out-of-sample financial evaluation on the Fama–French 49-industry daily-return data set used in the equity-data sanity check of Section 5.6.

Reconstruction. For each of the 90 direct-QPU portfolios saved in the equity-data campaign — 5 rolling rebalance windows (1927-05-31, 1951-12-31, 1976-08-31, 2001-04-30, 2025-12-31), each with $N \in \{10, 20, 30\}$, two topologies (Pegasus, Zephyr), and three chain strengths — we reconstruct the daily out-of-sample portfolio return as the equal-weight mean over the selected industries’ realised daily returns for the calendar month following the rebalance date. The five rebalance dates are chosen as evenly spaced indices over the 1,184 available monthly rebalance dates in 1926–2025. No daily-return data is required from the saved JSONL; only the saved selected-industries list and the public Kenneth French daily data [French, 2026].

Metrics. We report annualised Sharpe ratio (scaled by $\sqrt{252}$), max drawdown, Probabilistic Sharpe Ratio (PSR; Bailey and López de Prado, 2012), and Deflated Sharpe Ratio (DSR; Bailey and López de Prado, 2014) with the number of independent configurations per (window, N) cell as the deflation count. Because six configurations are tried per (window, N) cell (two topologies \times three chain strengths), DSR is computed with $N_{\text{trials}} = 6$ to discount the Sharpe for selection bias across configurations.

For comparison we compute the same metrics on the equal-weight all-49 industry portfolio (the $1/N$ baseline of DeMiguel et al., 2009) over the same five evaluation months. The $1/N$ baseline is widely understood to be a hard-to-beat benchmark in industry-level rolling allocation.

Aggregate result. Across all 90 QPU portfolios, the mean annualised Sharpe ratio is +1.94; on the same five evaluation months, the $1/N$ all-49 baseline delivers a mean Sharpe of +2.22. The QPU-selected portfolios *underperform* the $1/N$ baseline by a Sharpe delta of -0.28 on average.

This finding is consistent with the broad DeMiguel et al. [2009] result that $1/N$ is hard to beat with plug-in mean-variance allocations. The five-window breakdown (Table 8) is descriptive only — 5 rolling windows is too thin a sample for inferential claims about regime dependence — but it shows that the average underperformance is not uniform across the sampled period: the largest positive QPU-minus- $1/N$ spread occurs in window 0 (1927-06-01 through 1927-06-30, where the QPU-selected $N=10$ portfolio achieves Sharpe +1.29 while the $1/N$ baseline delivers -1.21), while in windows 1–4 the $1/N$ baseline meets or exceeds the QPU-selected portfolios.

Table 8: Out-of-sample annualised Sharpe ratio on the FF-49 evaluation months. “Mean QPU” is averaged over 6 configurations per (window, N) cell (2 topologies \times 3 chain strengths). “ $1/N$ baseline” is equal-weight over all 49 industries.

Window (rebalance date)	QPU N=10	QPU N=20	QPU N=30	$1/N$ baseline
0 (1927-05-31)	+1.29	+0.06	−0.98	−1.21
1 (1951-12-31)	+2.05	+2.64	+2.19	+2.20
2 (1976-08-31)	+0.72	+2.32	+2.07	+2.92
3 (2001-04-30)	−1.98	+0.74	+1.36	+1.85
4 (2025-12-31)	+4.05	+5.33	+7.29	+5.35
Mean over windows	+1.23	+2.22	+2.39	+2.22

Implication for the QF audience. The cardinality-constrained mean-variance-turnover problem class studied in this paper is solver-tractable to optimality (Gurobi proves optimum on all $N \leq 200$ tested instances; CQM matches Gurobi on all 54 head-to-head cases) but is not financially competitive against $1/N$ at the aggregate level on the FF-49 industry data set. The practical recommendation to a portfolio manager evaluating D-Wave hybrid solvers is therefore double-edged: the platform-internal CQM path is solver-equivalent to a Gurobi-optimal MIQP and reproduces the objective levels reachable by a classical Tabu heuristic at matched compute (Sections 5.5–5.9); the portfolios it returns underperform $1/N$ in Sharpe terms on average across the five sampled windows. For a rebalancing system with a 5 s decision cadence, the relevant operational question is not whether the QPU is doing the work, but whether the resulting portfolios are worth the entire pipeline’s operational and cloud cost; on the present data, the answer on the aggregate of the five evaluated windows is no.

6 Discussion

6.1 Formulation Choice Dominates Solver Choice

On the tested instance families, the constraint-native CQM formulation produces lower objective values than the penalty-encoded BQM formulation at every $N > 10$, across all three density families, and at every tested budget. The mechanism is clear: the penalty term $A \cdot \mathbf{1}\mathbf{1}^\top$ adds $O(N^2)$ couplers with magnitude A to the QUBO, while the economic signal in Σ is distributed across entries whose individual magnitudes diminish as N grows. At $N = 200$, the penalty dominates entirely. This is consistent with the constraint-dilution diagnosis of Lozano [2026], now confirmed in the hybrid setting.

6.2 Density Collapse as Structural Explanation

The density-axis collapse (Section 2.5) provides a structural explanation for the formulation gap. For direct QPU and hybrid BQM, the penalty term forces a complete logical graph regardless of the original Σ density. Chain-break fractions and embedding overheads at each N are virtually identical across diagonal, block, and dense families. For CQM, the original density is preserved, potentially allowing the hybrid solver’s classical component to exploit sparsity. This asymmetry means that density is a meaningful benchmark axis only for the CQM path.

6.3 CQM Budget Saturation

On the tested instances, the CQM solver returns identical solutions at 5 and 300 seconds. We interpret this cautiously: it indicates that the hybrid CQM solver’s internal classical-plus-quantum allocation reaches a stable point quickly for problems of this structure and scale ($N \leq 400$, binary variables, single equality constraint). It does not imply that CQM always converges in 5 seconds for richer constraint sets or non-binary variables.

6.4 Role of Direct QPU

Direct QPU access with penalty-encoded QUBOs is structurally disadvantaged for this problem class due to the fully-connected logical graph. At $N = 80$, embedding requires 750 physical qubits (9.4× overhead) and produces chain-break fractions above 0.93. For practitioners choosing within the D-Wave ecosystem, hybrid CQM offers better solution quality with no embedding or post-processing overhead. Direct QPU remains relevant for studying annealing dynamics and for problem classes with naturally sparse logical graphs.

6.5 Implications for Quantum Finance Benchmarks and Deployment

These results should temper the broad “quantum advantage in finance” narrative. The CQM path matches Gurobi on the tested instances, but Gurobi also proves optimality, so the result is a practical D-Wave deployment finding rather than a classical-superiority finding. The field-level implication is that quantum-finance evaluations can be dominated by modeling-interface choices: the same financial problem looks weak when the constraint is penalty-encoded as BQM and Gurobi-optimal when expressed as CQM. Future quantum-finance claims should therefore separate three questions: modeling fidelity (does the formulation faithfully represent the financial problem?), hybrid-solver usefulness (does the D-Wave workflow produce good solutions within operational time budgets?), and classical competitiveness (does the quantum-assisted path outperform strong classical alternatives?).

For financial institutions evaluating D-Wave, the immediate recommendation is to prototype constrained portfolio and allocation problems in CQM first, measure against a strong MIQP baseline, and avoid treating QUBO penalty tuning as the default production route. This is especially relevant to prediction-market optimization systems and market venues where portfolio selection over bets or contracts combines cardinality, exposure limits, budget constraints, and turnover costs.

A second deployment-relevant consequence comes from the budget-saturation result of Section 5.7. For periodic-rebalancing systems with a decision cadence on the order of the hybrid solver’s 5s minimum or longer (intraday sector-rotation engines, end-of-period portfolio re-allocation, batch contract-basket re-sizing, or any periodic re-optimization over many simultaneously open events or contracts), the relevant operational metric is not per-call quality at unbounded budget, but the quality reachable within the shortest acceptable budget. On the tested instances the CQM service returns the same solution at the 5s minimum and at every longer budget up to 300s, and the same solution across repeated calls. In a system where the rebalancing rate, not per-call solve time, is the binding constraint, the orchestrator’s decision collapses to “how often to re-solve?” rather than “how long to wait?”, and budget tuning ceases to be a system-level parameter. We deliberately exclude latency-critical execution paths (sub-second in-play markets, microsecond execution venues) from this discussion: a 5s minimum solve time is incompatible with those use cases regardless of solution quality. The penalty-encoded BQM path admits no analogous guarantee on the tested instances at any tested budget.

6.6 Scope and Limitations

This study compares formulations and solver interfaces within the D-Wave platform. It is not a general quantum-vs-classical benchmark: Gurobi MIQP solves all tested instances at $N \leq 200$ to proven optimality in under 300 seconds, and we make no claim that any D-Wave path is competitive with state-of-the-art classical solvers on this problem class.

Additional limitations:

- The penalty weight $A = 4.0$ is held fixed following the calibration of Lozano [2026]; Appendix A verifies robustness to $A \in \{2, 4, 8\}$ but does not perform a full per-instance sweep.
- The real-data section uses only $N \leq 30$; it serves as a directional sanity check, not as the primary evidence.
- Warm-start / reverse-annealing experiments are deferred to future work.
- Richer constraint sets (sector exposure caps, ESG exclusions, mutual exclusivity, and multi-period turnover budgets) would test whether the CQM advantage persists under institutional-grade complexity. Prediction-market and sports-betting allocation, where a

trader selects a limited number of contracts subject to budget and rebalancing costs, provides a natural sparse-graph extension.

- Stochastic validation (10 repetitions) is performed on a representative subset; the full grid is single-shot per configuration.

7 Conclusion

We have audited where the quantum contribution actually lives in D-Wave’s hybrid quantum-classical service for cardinality-constrained portfolio selection with switching costs. The headline observation is structural: the constraint-native LeapHybridCQM service matches Gurobi’s proven optimum on all 54 head-to-head instances at $N \leq 120$, but the mean QPU access time is 0.034 s out of a 5 s wall-clock budget, roughly 0.7% of the run (precise: 0.68%, 0.034/5.0). The remaining $\sim 99\%$ is the service’s classical decomposition, sub-problem assembly, and feasibility-aware reassembly. At the level of reported service telemetry, the observed D-Wave hybrid win on this problem class is therefore dominated by classical hybrid orchestration with a small measured QPU-access component; the CPU-only counterfactual of Section 5.9 bounds the causal QPU share from above empirically: at matched 5 s wall-clock, a classical heuristic on the penalty-encoded BQM reproduces hybrid CQM’s objective levels to within mean absolute delta 0.001 on 24 tested instances. A true internal sub-solver ablation of the LeapHybridCQM pipeline — replacing the QPU sub-call with a classical sub-solver inside D-Wave’s proprietary decomposition workflow — remains future work requiring vendor cooperation. Three further results sharpen this audit:

1. The cardinality penalty contributes a dense rank-one matrix that makes the penalty-encoded logical graph fully connected regardless of covariance density, collapsing the density benchmark axis for all penalty-encoded paths (BQM and direct QPU).
2. The CQM service returns bitwise-identical objective values (zero variance to floating-point precision) at every tested wall-clock budget from 5 to 300 seconds and across repeated calls, eliminating budget tuning as a design variable on this problem class.
3. Constraint-native CQM produces lower objective values than the penalty-encoded BQM interface at every tested $N > 10$ across all density families, extending prior work on CQM-vs-BQM constraint handling with a Gurobi MIQP optimality anchor and showing that the BQM degradation is a formulation effect rather than a solver-specific artifact (simulated annealing applied to the same BQM exhibits the same degradation; a paired Wilcoxon signed-rank test rejects $H_0 : f_{\text{CQM}} = f_{\text{BQM}}$ at every $N \geq 20$, $p < 0.05$).

For practitioners using D-Wave hybrid solvers, these results recommend the constraint-native CQM interface and, more importantly, change how D-Wave hybrid performance should be reported. A reported "hybrid win" carries no automatic implication that the QPU is doing material work; the quantum contribution must be measured and disclosed alongside the wall-clock and quality numbers. We propose that future quantum-finance benchmarks report `run_time`, `charge_time`, and `qpu_access_time` separately, together with the QPU-fraction of wall-clock, so that the quantum-versus-classical attribution of any reported advantage is unambiguous.

Data and Code Availability

Synthetic instances are generated from parametric covariance models with fixed random seeds for reproducibility. Equity returns are from the Kenneth French Data Library, 49 industry portfolios, daily [French, 2026]. Source code for all experiments (QUBO/CQM construction, solver wrappers, analysis scripts, audit-protocol reference implementation), random seeds, solver

configurations, and processed result JSONLs are publicly available under the MIT License at <https://github.com/LuisLozanoM/where-quantum-lives>. The Wilcoxon, dwell-vs-quality, and Table 5 cell-level verification scripts referenced in this paper live under `analysis/` in that repository.

Acknowledgments

We thank the D-Wave team for providing access to quantum computing resources through the Leap cloud platform and for their continuous technical support. Live QPU experiments used `Advantage_system4.1` (Pegasus) and `Advantage2_system1.13` (Zephyr).

Statements and Declarations

Competing Interests

I declare no competing interests.

Funding

This research received no external funding. QPU access was obtained through my personal D-Wave Leap cloud subscription.

Authors' Contributions

I am the sole author and conceived the study, designed the experiments, implemented the code, ran the experiments, analyzed the results, and wrote the manuscript.

AI Assistance Disclosure

I used AI-based coding assistants and editorial tools for code scaffolding and language support; all experimental design, verification, analysis, and final manuscript decisions were my own.

A Penalty Robustness Check

The penalty weight $A = 4.0$ used in the main experiments is consistent with the calibration study of Lozano [2026]. We verify that the BQM results are not artifacts of a single penalty value by running the hybrid BQM solver at $A \in \{2, 4, 8\}$ on a subset of 12 instances ($N \in \{20, 50, 80, 120\}$, all three density families, seed 0).

Table 9 reports the projected objective values. All 36 runs returned raw-feasible solutions (the hybrid solver satisfied the penalty-encoded cardinality constraint before post-processing in every case). The objective values are qualitatively similar across penalty values at each (N, ρ) , with no systematic trend favoring any particular A . The BQM degradation at large N is present at all three penalty levels, confirming that it is a structural consequence of the fully-connected penalty term rather than a tuning artifact.

Table 9: Hybrid BQM objective by penalty weight A (projected to exact- K). All 36 runs returned raw-feasible solutions. Objective values are qualitatively stable across A .

N	Family	$A = 2$	$A = 4$	$A = 8$
20	diagonal	-0.340	-0.340	-0.340
50	diagonal	-0.587	-0.603	-0.590
80	diagonal	-0.929	-0.931	-0.910
120	diagonal	-1.239	-1.155	-1.181
20	block	-0.252	-0.252	-0.264
50	block	-0.348	-0.361	-0.395
80	block	-0.059	-0.069	-0.040
120	block	+0.909	+1.003	+0.982
20	dense	-0.365	-0.365	-0.350
50	dense	-0.672	-0.677	-0.693
80	dense	-1.119	-1.093	-1.060
120	dense	-1.613	-1.462	-1.453

References

- Atithi Acharya, Romina Yalovetzky, Pierre Minssen, Shouvanik Chakrabarti, Ruslan Shaydulin, Rudy Raymond, Yue Sun, Dylan Herman, Ruben S. Andrist, Grant Salton, Martin J. A. Schuetz, Helmut G. Katzgraber, and Marco Pistoia. Decomposition pipeline for large-scale portfolio optimization with applications to near-term quantum computing. *Physical Review Research*, 7:023142, 2025. doi: 10.1103/PhysRevResearch.7.023142.
- David H. Bailey and Marcos López de Prado. The Sharpe ratio efficient frontier. *Journal of Risk*, 15(2):3–44, 2012.
- David H. Bailey and Marcos López de Prado. The deflated Sharpe ratio: Correcting for selection bias, backtest overfitting, and non-normality. *Journal of Portfolio Management*, 40(5):94–107, 2014. doi: 10.3905/jpm.2014.40.5.094.
- Dimitris Bertsimas and Romy Shioda. Algorithm for cardinality-constrained quadratic optimization. *Computational Optimization and Applications*, 43(1):1–22, 2009. doi: 10.1007/s10589-007-9126-9.
- Kelly Boothby, Paul Bunyk, Jack Raymond, and Aidan Roy. Next-generation topology of D-Wave quantum processors. 2020. doi: 10.48550/arXiv.2003.00133. Pegasus and Zephyr topology design and embedding constants.
- Giuseppe Buonaiuto, Francesco Gargiulo, Giuseppe De Pietro, Massimo Esposito, and Marco Pota. Best practices for portfolio optimization by quantum computing, experimented on real quantum devices. *Scientific Reports*, 13:19434, 2023. doi: 10.1038/s41598-023-45392-w.
- D-Wave Systems. Hybrid solver service, 2025a. URL https://docs.dwavequantum.com/en/latest/quantum_research/hybrid.html. Accessed April 7, 2026.
- D-Wave Systems. Hybrid solver service: Documentation and timing fields, 2025b. URL https://docs.dwavequantum.com/en/latest/quantum_research/hybrid.html. Defines `run_time`, `charge_time`, and `qpu_access_time` for the LeapHybridCQM and LeapHybridBQM samplers; accessed 2026-05-31.
- Victor DeMiguel, Lorenzo Garlappi, and Raman Uppal. Optimal versus naive diversification: How inefficient is the $1/N$ portfolio strategy? *Review of Financial Studies*, 22(5):1915–1953, 2009. doi: 10.1093/rfs/hhm075.
- Kenneth R. French. 49 industry portfolios, 2026. URL https://mba.tuck.dartmouth.edu/pages/faculty/ken.french/Data_Library/det_49_ind_port.html. Accessed March 31, 2026.
- Dylan Herman, Cody Googin, Xiaoyuan Liu, Yue Sun, Alexey Galda, Ilya Safro, Marco Pistoia, and Yuri Alexeev. Quantum computing for finance. *Nature Reviews Physics*, 5(8):450–465, 2023. doi: 10.1038/s42254-023-00603-1.
- Jonas Lang, Sebastian Zielinski, and Sebastian Feld. Strategic portfolio optimization using simulated, digital, and quantum annealing. *Applied Sciences*, 12(23):12288, 2022. doi: 10.3390/app122312288.
- Luis Lozano. A penalty-free pipeline for direct quantum-annealer portfolio optimization, 2026. URL <https://arxiv.org/abs/2605.17628>.
- Andrew Lucas. Ising formulations of many NP problems. *Frontiers in Physics*, 2:5, 2014. doi: 10.3389/fphy.2014.00005.

- Harry Markowitz. Portfolio selection. *The Journal of Finance*, 7(1):77–91, 1952. doi: 10.2307/2975974.
- Sai Nandan Morapakula, Sangram Deshpande, Rakesh Yata, Rushikesh Ubale, Uday Wad, and Kazuki Ikeda. End-to-end portfolio optimization with hybrid quantum annealing. *Advanced Quantum Technologies*, 2025. doi: 10.1002/qute.202500753.
- Samuel Mugel, Carlos Kuchkovsky, Escolástico Sánchez, Samuel Fernández-Lorenzo, Jorge Luis-Hita, Enrique Lizaso, and Román Orús. Dynamic portfolio optimization with real datasets using quantum processors and quantum-inspired tensor networks. *Physical Review Research*, 4:013006, 2022. doi: 10.1103/PhysRevResearch.4.013006.
- Román Orús, Samuel Mugel, and Enrique Lizaso. Quantum computing for finance: Overview and prospects. *Reviews in Physics*, 4:100028, 2019. doi: 10.1016/j.revip.2019.100028.
- Elijah Pelofske. Comparing three generations of D-Wave quantum annealers for minor embedded combinatorial optimization problems. *Quantum Science and Technology*, 10(2):025025, 2025. doi: 10.1088/2058-9565/adb029.
- Wolfgang Sakuler, Johannes M. Oberreuter, Riccardo Aiolfi, Luca Asproni, Branislav Roman, and Jürgen Schiefer. A real-world test of portfolio optimization with quantum annealing. *Quantum Machine Intelligence*, 7:43, 2025. doi: 10.1007/s42484-025-00268-2.
- Davide Venturelli and Alexei Kondratyev. Reverse quantum annealing approach to portfolio optimization problems. *Quantum Machine Intelligence*, 1:17–30, 2019. doi: 10.1007/s42484-019-00001-w.
- Amit Verma and Mark Lewis. Penalty and partitioning techniques to improve performance of QUBO solvers. *Discrete Optimization*, 44:100594, 2022. doi: 10.1016/j.disopt.2020.100594.